High-Frequency Resonance Analysis and Reshaping Control Strategy of DFIG System Based on DPC

Bin Hu, Heng Nian, *Senior Member, IEEE*, Jun Yang, Meng Li, and Yunyang Xu, *Graduate Student Member, IEEE*

***Abstract*—Direct power control (DPC) can reduce the complexity of a controller and enhance the dynamic response for doubly fed induction generators (DFIG) system. The high-frequency resonance (HFR) issues will be analyzed for the DFIG system based on DPC under inductive weak grid in this article. Based on the simplified high-frequency impedance model of the DFIG system based on DPC and the Bode diagram of equivalent single-input single-output impedance, it is found that a strong frequency coupling related to the components of system delay in off-diagonal admittance will cause the high-frequency phase to change periodically for the DFIG system. Therefore, the DFIG system will show capacitive or even negative resistance to introduce potential risk of HFR at high frequency. The stability of a DFIG system will be further deteriorated as the system delay increases. An impedance reshaping control strategy is proposed to reduce the degree of frequency coupling at high frequency for eliminating the negative effects of system delay, so that HFR can be suppressed. The experimental results validate the availability of the proposed reshaping control strategy.**

***Index Terms*—Direct power control (DPC), doubly fed induction generator (DFIG), frequency coupling, high-frequency resonance (HFR), virtual impedance.**

I. Introduction

With the gradually increasing number of renewable energy generation systems in the power grid, the doubly fed induction generator (DFIG) has been widely utilized in practice for the small converter rating, low cost, and competitive durability [1], [2]. The installation capacity of a DFIG system continues to grow as the penetration of renewable energy increases [3].

The DFIG-based wind energy conversion systems are usually operated in the offshore or mountainous regions, indicating that the DFIG system is always connected to the weak power grid with low short circuit ratio (SCR) [4]–[7]. There are some resonance issues under weak grid for a DFIG system, which can be categorized into sub- and supersynchronous resonance (SSR) and high-frequency resonance (HFR) [8]–[10]. The impedance-based methods can be carried out to analyze these resonance issues under weak grid [11]–[13].

It has been reported that the SSR is closely related to the control strategy of a DFIG system. For example, the phase-locked loop (PLL) will introduce the negative resistance around the fundamental frequency when the bandwidth of the PLL is too large, which will deteriorate the stability of DFIG system under inductive weak grid and cause the SSR [14], [15]. In addition, SSR will also exist in the DFIG system with series-compensated power networks, due to the subsynchronous control interaction (SSCI) [16].

Compared with the SSR, the HFR is mainly related to the passive impedance characteristics mismatch of a DFIG system and weak grid, since the effect of controllers can be ignored at high frequency [17]. One of the HFR is that the DFIG system always behaves as an inductance at high frequency, and has insufficient phase margin when connected to the parallel-compensated grid, which is capacitive at high frequency [17]. Another scenario of HFR occurs in the voltage source converter based high-voltage direct current transmission whose phase is below –90° in some region at high frequency [18], [19], thereby mismatching the inductive characteristic of a DFIG system.

It should be noted that in the analysis on the above-mentioned HFR issues, DFIG always employs the conventional vector control that contains the inner-loop current regulator and outer-loop power regulator [10]. Various direct power control (DPC) methods for DFIG systems are proposed to avoid the current regulator, such as the sliding mode control (SMC) DPC [20], model predictive control (MPC) DPC [21], and grid voltage modulated (GVM) DPC [22], [23]. However, since the fast dynamic power tracking ability of DPC may affect the high-frequency characteristics, it is important to analyze whether the DPC strategy will influence the stability of a DFIG system at high frequency to cause HFR. The similarity of these three types of DPC is that the active power and reactive power can be directly controlled to reduce the complexity of controller and enhance the dynamic response [24]. This article first selected the proportional integral (PI) DPC for analysis that can output the reference power based on PLL and the PI controller, because this type of DPC is very representative. The PI-DPC appearing in the remaining article will be replaced by DPC for simplicity.

Hu *et al.* [25] established the impedance model of DFIG system based on DPC to analyze the impedance characteristics under inductive weak grid. It can be found that there is a strong

Manuscript received August 6, 2020; revised October 22, 2020 and November 25, 2020; accepted December 15, 2020. Date of publication December 18, 2020; date of current version March 5, 2021. This work was supported by the National Natural Science Foundation of China under Grant 51977194. Recommended for publication by Associate Editor M. S. ElMoursi. *(Corresponding author: Heng Nian.)*

The authors are with the College of Electrical Engineering, Zhejiang University, Hangzhou 310058, China (e-mail: 11810031@zju.edu.cn; nianheng@zju.edu.cn; johniej@zju.edu.cn; 11910042@zju.edu.cn; xuyunyang@zju.edu.cn).

Color versions of one or more figures in this article are available at https://doi.org/10.1109/TPEL.2020.3045860.

Digital Object Identifier 10.1109/TPEL.2020.3045860

frequency coupling characteristic in the developed impedance model, indicating that the impedance model of a DFIG system based on DPC is a multiple-input multiple-output (MIMO) model with coupled positive and negative sequence impedance [26]. The frequency coupling characteristic will complicate the impedance analysis, and there will be an additional resonance component that differs by 100 Hz when the DFIG-grid interconnected system oscillates [27]. It still needs to investigate that whether this strong frequency coupling will cause some potential risk of HFR at high frequency.

Furthermore, the research works in [9] and [17] proposed a damping method and a virtual impedance to suppress the HFR and enhance the stability of a DFIG system connected with parallel compensation grid. However, the existing high-frequency impedance reshaping control strategies all ignore the frequency coupling since the impedance characteristic of DFIG system based on conventional vector control strategy is a single-input single-output (SISO) model at high frequency [15]. It is of importance to propose an improved impedance reshaping control strategy when the HFR occurs in a MIMO system, such as a DFIG system based on DPC. Moreover, the system delay cannot be neglected at high frequency when the large bandwidth of a power controller is employed [17], it should pay more attention whether the system delay will affect the impedance characteristics of a DFIG system based on DPC to degrade the system stability.

This article establishes a simplified impedance model of a DFIG system with DPC at high frequency. Based on the equivalent SISO impedance model, the high-frequency impedance characteristics are analyzed and it can be seen that the system delay will deteriorate the phase margin at high frequency for the DFIG system. Considering the limitation of the existing system delay compensation strategy, this article studies the impedance subsystem that considers the frequency coupling to further analyze the high-frequency impedance characteristics, then an improved impedance reshaping control strategy is designed in this article.

The rest of this article is organized as follows. Section II describes the DFIG system configuration and discovers the resonance issues based on DPC. The simplified high-frequency impedance model is developed in Section III. Section IV validates the proposed impedance model, then studies the equivalent SISO impedance model and the existing system delay compensation strategy. Further analysis of high-frequency characteristics and reshaping control strategy are proposed in Section V. Section VI gives the experiment results to verify the correctness of the proposed reshaping control strategy. Finally, Section VII summarizes the conclusion.

II. DFIG System Configuration and Resonance Issues Based on DPC

The DFIG system can achieve the maximum power point tracking and the stable dc voltage by employing the rotor side converter (RSC) and the grid side converter (GSC), respectively. The overall impedance of a DFIG system can be regarded as the parallel connection of DFIG+RSC and GSC. Since the GSC has less effect on impedance characteristics due to limited slip power, this article only considers the impedance of DFIG+RSC at high frequency. The detailed control equation of DPC can be written as [24]

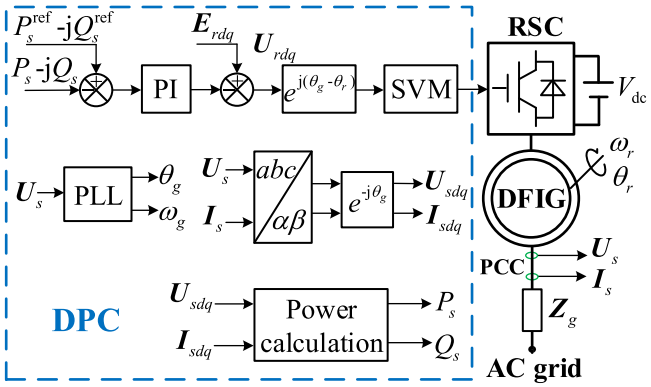

Fig. 1. Topology and control diagram of DFIG+RSC based on DPC.

$$\boldsymbol{U}_{rdq} = \boldsymbol{E}_{rdq} - \frac{2\boldsymbol{U}_{sdq}}{U_s^2}\left(\frac{R_s L_r + R_r L_s}{3L_m} + \frac{\sigma L_s L_r}{L_m}\frac{d}{dt}\right)\boldsymbol{S}_s \tag{1}$$

$$\boldsymbol{E}_{rdq} = \frac{L_r}{L_m}\left[\boldsymbol{U}_{sdq} + \left(\frac{R_r}{L_r} - \mathrm{j}\omega_r\right)\boldsymbol{\psi}_{sdq} - \frac{2j\omega_g \sigma L_s \boldsymbol{U}_{sdq}\boldsymbol{S}_s}{3U_s^2}\right] \tag{2}$$

where the bold letters are used in this article to denote complex space vectors or 2×2 matrix. U, I, Ψ, P, and Q denote the voltage, current, flux linkage, active power, and reactive power, respectively. The subscripts s and r denote the stator and rotor parameters. The subscripts d and q denote the d- and q-axis components in the rotating reference frame. $\boldsymbol{E}_{rdq}$ denotes the decoupling voltage component. ω_g and ω_r are the grid angular frequency and the rotor angular frequency. $\boldsymbol{S}_s = P_s - jQ_s$ is the complex power. R_s and R_r are the stator and rotor resistances. $L_s = L_m + L_{ls}$ and $L_r = L_m + L_{lr}$ are the self-inductances of stator and rotor windings. L_{ls}, L_{lr}, and L_m are the stator and rotor leakage inductances and mutual inductance, and $\sigma = 1 - L_m^2/(L_s \cdot L_r)$.

According to (1) and (2), the topology and control diagram of DFIG+RSC based on DPC can be shown in Fig. 1. The superscript ref denotes the reference value. The dc-link voltage V_{dc} is assumed to be constant. $\boldsymbol{Z}_g$ is the grid impedance. The stator voltage $\boldsymbol{U}_s$ and stator current $\boldsymbol{I}_s$ are sampled from the point of common coupling. The grid angle θ_g and grid angular frequency ω_g are obtained by PLL. The rotor angular frequency ω_r and rotor angle θ_r are obtained by the encoder.

Since the control effect of controllers and its delay time always can be ignored above the control bandwidth for conventional vector control, the impedance characteristics of the DFIG system based on vector control are dominated by its passive components, in which the DFIG system will behave as an inductance and have enough phase margin under inductive weak grid at high frequency [15].

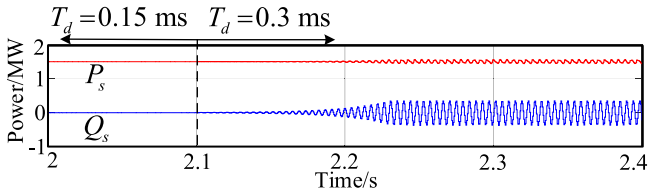

Fig. 2. Resonance phenomenon of DFIG based on DPC.

However, if DPC is employed in DFIG control, it can be found that, when the system delay time T_d increases from 0.15 to 0.3 ms at 2.1 s according to Fig. 2, the DFIG-grid interconnected system has some resonance issues at high frequency. Therefore, the system delay may influence the stability of the DFIG system based on DPC, to cause the DFIG system not always an inductance at high frequency.

III. Impedance Modeling of DFIG Based on DPC at High Frequency

Based on impedance-based method, the small-signal models of DFIG and RSC are established, then the simplified impedance model of a DFIG system based on DPC at high frequency can be obtained in Section III-C. The HFR issues for a DFIG system with DPC under inductive weak grid can be analyzed by the developed impedance model.

A. Small-Signal Model of DFIG

The voltage and flux linkages in the stationary coordinate system can be shown as

$$\begin{cases} \boldsymbol{U}_s = R_s \boldsymbol{I}_s + s\boldsymbol{\psi}_s \\ \boldsymbol{U}_r = R_r \boldsymbol{I}_r + s\boldsymbol{\psi}_r - \mathrm{j}\omega_r \boldsymbol{\psi}_r \end{cases} \tag{3}$$

$$\begin{cases} \boldsymbol{\psi}_s = L_s \boldsymbol{I}_s + L_m \boldsymbol{I}_r \\ \boldsymbol{\psi}_r = L_m \boldsymbol{I}_s + L_r \boldsymbol{I}_r. \end{cases} \tag{4}$$

The rotor voltage can be rewritten according to (3) and (4)

$$\boldsymbol{U}_r = \left[R_r + (s - j\omega_r) L_r \sigma\right] \boldsymbol{I}_r + (s - j\omega_r) \frac{L_m}{L_s} \boldsymbol{\psi}_s. \tag{5}$$

After combining (3)–(5) to eliminate the rotor current and stator flux linkage, the positive and negative sequence-domain equations of DFIG, which ignores the stator resistance, are expressed as

$$\begin{bmatrix} I_{sp} \\ I_{sn} \end{bmatrix} = \left(\frac{1}{L_s} \boldsymbol{G}_1 + \frac{L_m}{L_s} \boldsymbol{G}_1 \boldsymbol{G}_2 \boldsymbol{G}_3 \right) \begin{bmatrix} U_{sp} \\ U_{sn} \end{bmatrix} - \frac{L_m}{L_s} \boldsymbol{G}_3 \begin{bmatrix} U_{rp} \\ U_{rn} \end{bmatrix} \tag{6}$$

$$\boldsymbol{G}_1 = \begin{bmatrix} \frac{1}{s} & 0 \\ 0 & \frac{1}{s-2j\omega_g} \end{bmatrix} \boldsymbol{G}_2 = \frac{L_m}{L_s} \begin{bmatrix} s - j\omega_r & 0 \\ 0 & s + j\omega_r - 2j\omega_g \end{bmatrix}$$

$$\boldsymbol{G}_3 = \begin{bmatrix} \frac{1}{R_r + (s - j\omega_r) L_r \sigma} & 0 \\ 0 & \frac{1}{R_r + (s + j\omega_r - 2j\omega_g) L_r \sigma} \end{bmatrix} \tag{7}$$

where subscripts p and n denote the positive and negative sequence components. The negative sequence equation is obtained by moving twice grid angular frequency $2\omega_g$ from positive sequence equation and reversing rotor angular frequency ω_r. The positive and negative sequence are two independent subsystems when the RSC is not considered since the matrices $\boldsymbol{G}_1$, $\boldsymbol{G}_2$, and $\boldsymbol{G}_3$ are all diagonal matrices.

B. Small-Signal Model of RSC

The influence of PLL can be ignored at high frequency due to the limited control bandwidth [17]. The active power and reactive power can be controlled directly by DPC, and the power calculation can be expressed as

$$\begin{cases} P_s = 1.5(I_{sd} U_{sd} + I_{sq} U_{sq}) \\ Q_s = 1.5(-I_{sd} U_{sq} + I_{sq} U_{sd}). \end{cases} \tag{8}$$

Since $\boldsymbol{U}_{sdq}$ is aligned to the d-axis when employing the PLL, there is no steady-state stator voltage in the q-axis, i.e., $\boldsymbol{U}_{sdq1} = U_{sd1} + j0$, in which subscript 1 denotes the steady-state component. According to (8) and the transformation matrix between dq domain and sequence domain [12], the small-signal equation of rotor voltage in sequence domain can be expressed as

$$\begin{bmatrix} \Delta U_{rp} \\ \Delta U_{rn} \end{bmatrix} \approx \boldsymbol{G}_{PQ} \left(\boldsymbol{G}_{pnu} \begin{bmatrix} \Delta I_{sp} \\ \Delta I_{sn} \end{bmatrix} + \boldsymbol{G}_{pni} \begin{bmatrix} \Delta U_{sp} \\ \Delta U_{sn} \end{bmatrix} \right) \tag{9}$$

$$\boldsymbol{G}_{pnu} = \begin{bmatrix} 1.5U_{sd1} & 0 \\ 0 & 1.5U_{sd1} \end{bmatrix} \boldsymbol{G}_{pni} = \begin{bmatrix} 0 & 1.5\boldsymbol{I}_{s1} \\ 1.5\boldsymbol{I}_{s1}^* & 0 \end{bmatrix} \tag{10}$$

$$\boldsymbol{G}_{PQ} = \begin{bmatrix} H_{pi}(s) & 0 \\ 0 & H_{pi}(s) \end{bmatrix} = \begin{bmatrix} \frac{K_p(s - j\omega_g) + K_i}{s - j\omega_g} & 0 \\ 0 & \frac{K_p(s - j\omega_g) + K_i}{s - j\omega_g} \end{bmatrix} \tag{11}$$

where Δ denotes the small-signal component. $*$ denotes the conjugate operator. The steady-state stator current $\boldsymbol{I}_{s1} = I_{sd1} + \mathrm{j}I_{sq1}$. $\boldsymbol{G}_{pnu}$ and $\boldsymbol{G}_{pni}$ are the parameter matrix of stator voltage and stator current, respectively. K_p and K_i are, respectively the proportional gain and integral gain of the power controller. Note that this article focuses on the stability of a DFIG system under the inductive weak grid, thus the decoupling voltage component $\boldsymbol{E}_r$ in (1), which can enhance the dynamic performance of the DPC under asymmetric voltage faults, will not be considered in the impedance modeling.

C. Impedance Model of a DFIG System at High Frequency

According to Sections III-A and III-B, Fig. 3 depicts the impedance model of DFIG based on DPC. The symbol "Δ" is omitted for simplicity.

In Fig. 3, $\boldsymbol{K}_m$ represents the system delay matrix, in which the delay time T_d is always equal to 1.5 times the switching period $1/f_s$ [15]

$$\boldsymbol{K}_m = \begin{bmatrix} e^{-sT_d} & 0 \\ 0 & e^{-(s-2j\omega_g)T_d} \end{bmatrix}. \tag{12}$$

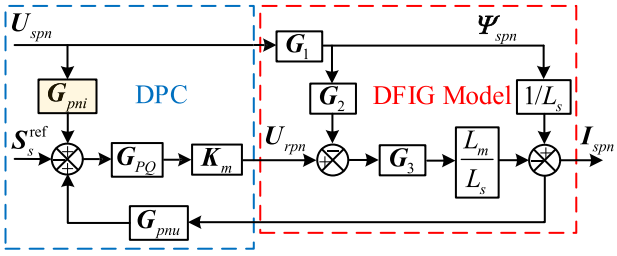

Fig. 3. DFIG impedance model based on DPC.

TABLE I
PARAMETERS OF DFIG

Parameter	Value	Parameter	Value
Rated voltage U_s	690 V	Stator leakage L_{ls}	0.06 mH
Rated power P_s	1.5 MW	Rotor leakage L_{lr}	0.083 mH
Fundamental frequency f_1	50 Hz	Mutual inductance L_m	4.425 mH
Rotor frequency f_r	60 Hz	Turns ratio K_e	0.33
Pole pairs n_p	2	Switching frequency f_s	5 kHz
Dc-link voltage V_{dc}	1050 V	Delay time T_d	0.3 ms
Stator resistance R_s	2.4 mΩ	Proportional gain K_p	1.2
Rotor resistance R_r	2 mΩ	Integral gain K_i	6

According to Fig. 3, L_m can be approximated to L_s. The PI controller of power loop will degenerate into a proportional controller above the fundamental frequency, i.e., $H_{\rm pi}(s)\approx K_p$, and the DFIG parameter matrices can be simplified at high frequency, i.e., $\boldsymbol{G}_1/L_s\approx 0$ and $\boldsymbol{G}_3\cdot\boldsymbol{G}_2\approx 1/L_r\sigma$. Therefore, the admittance of the DFIG system based on DPC at high frequency can be simplified as

$$\boldsymbol{Y}_{\rm DFIG}=\frac{\boldsymbol{I}_{spn}}{\boldsymbol{U}_{spn}}=\begin{bmatrix}Y_{11} & Y_{12}\\ Y_{21} & Y_{22}\end{bmatrix}\approx(\boldsymbol{I}+\boldsymbol{G}_3\boldsymbol{K}_m\boldsymbol{G}_{PQ}\boldsymbol{G}_{pnu})^{-1}\left(-\boldsymbol{G}_3\boldsymbol{K}_m\boldsymbol{G}_{PQ}\boldsymbol{G}_{pni}+\frac{1}{L_r\sigma}\boldsymbol{G}_1\right) \tag{13}$$

$$\begin{cases}Y_{11}=\dfrac{(s-j\omega_r)/s}{(s-j\omega_r)L_r\sigma+1.5U_{sd1}K_pe^{-sT_d}}\\ Y_{12}=\dfrac{-1.5K_p\boldsymbol{I}_{s1}e^{-sT_d}}{(s-j\omega_r)L_r\sigma+1.5U_{sd1}K_pe^{-sT_d}}\\ Y_{21}=\dfrac{-1.5K_p\boldsymbol{I}_{s1}^*e^{-(s-2j\omega_g)T_d}}{(s+j\omega_r-2j\omega_g)L_r\sigma+1.5U_{sd1}K_pe^{-(s-2j\omega_g)T_d}}\\ Y_{22}=\dfrac{(s+j\omega_r-2j\omega_g)/(s-2j\omega_g)}{(s+j\omega_r-2j\omega_g)L_r\sigma+1.5U_{sd1}K_pe^{-(s-2j\omega_g)T_d}}.\end{cases} \tag{14}$$

IV. IMPEDANCE MODEL VERIFICATION AND ANALYSIS

A. Impedance Model Verification

The simulation model of a DFIG system based on DPC under inductive weak grid is developed in MATLAB/Simulink and the parameters are shown in Table I. The analytical models of DFIG based on DPC match the simulation results well as shown in Fig. 4, which validates the correctness of the proposed impedance model. Also, this impedance model has less parameter dependence, which is also accurately with DFIG parameters variations.

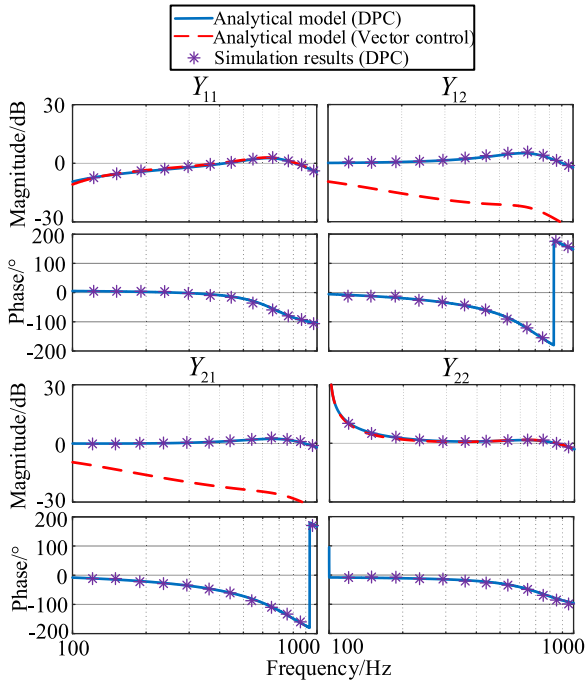

Fig. 4. Validation of DFIG impedance models based on DPC.

Since the bandwidth of inner-loop current controller is much greater than the bandwidth of outer-loop power controller for conventional vector control, the influence of the impedance characteristic for outer-loop power controller can be ignored compared with that of the inner-loop current controller. However, the power controller for DPC may dominate the impedance characteristic due to the lack of the inner-loop current controller and the large bandwidth of power controller. Therefore, the impedance characteristic of the DFIG system based on DPC is different from conventional vector control.

The amplitude–frequency characteristic curves of conventional vector control are also depicted in Fig. 4. The proportional gain K_p and the integral gain K_i for the current controller of conventional vector control and the power controller of DPC are the same. It should be noted that the frequency coupling characteristic around the fundamental frequency always exists due to the asymmetrical structure of PLL [15], whereas the DFIG system with conventional vector control can ignore the frequency coupling characteristic at high frequency, since the influence of PLL is weaken above the control bandwidth. Nevertheless, as for the DPC, it can be found that the value of amplitude–frequency characteristic curves in off-diagonal elements Y_{12} and Y_{21} is not smaller than diagonal elements Y_{11} and Y_{22} above 100 Hz, indicating that the DFIG impedance is also a MIMO model at high frequency with strong frequency coupling characteristics, which may increase the complexity of impedance analysis due to coupled positive and negative sequence impedances [26].

According to [28], to reduce the influence of harmonic distortion on the control effect, a bandpass filter is adopted in GVM-DPC. The harmonic components in the voltage input are filtered, thus the voltage input can be approximated as a dc value, which means the off-diagonal matrix $\boldsymbol{G}_{pni}$ will not be

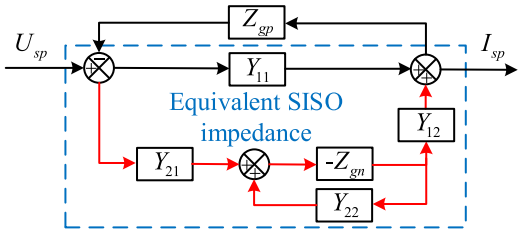

Fig. 5. Equivalent SISO impedance of a DFIG system.

considered at high frequency and there is no frequency coupling in GVM-DPC.

B. Equivalent SISO Impedance Model Analysis

It is difficult to describe the impedance characteristic and analyze the potential instability risks for a MIMO impedance model. Zhang *et al.* [27] proposed an equivalent SISO impedance model by loop decomposition method, which can facilitate the analysis of the impedance model as shown in Fig. 5. According to Fig. 5, the equivalent SISO impedance Z_{SISO} can be decomposed into the impedance subsystems Z_0 and Z_{cou} which is shown as follows:

$$Z_{SISO} = (1/Z_0 + 1/Z_{\mathrm{cou}})^{-1} \tag{15}$$

$$\begin{cases} Z_0 = 1/Y_{11} \\ Z_{\mathrm{cou}} = -(1 + Y_{22}Z_{gn})/(Y_{12}Z_{gn}Y_{21}) \end{cases} \tag{16}$$

where Z_0 is the DFIG impedance subsystem that ignores the frequency coupling characteristic, and Z_{cou} is the impedance subsystem introduced by frequency coupling characteristics that contains DFIG system admittance and negative sequence grid impedance $Z_{gn} = (s\text{-}2j\omega_g)L_g$, in which L_g denotes the grid inductance.

The stability margin of the DFIG system can be obtained by the Bode diagram with the positive sequence impedance of grid $Z_{gp} = sL_g$ and the equivalent SISO impedance for DFIG. Fig. 6 depicts the Bode diagram of equivalent SISO impedance for DFIG based on DPC. It can be seen that when the delay time T_d is 0.3, 0.15, and 0.075 ms, the amplitude–frequency characteristic curves of the equivalent SISO impedance for DFIG and the grid impedance intersect at 275, 382, and 562 Hz, respectively. The phase of the intersections is significantly reduced, in which the DFIG will be more capacitive as the switching frequency decreases. When the delay time $T_d = 0.3$ ms, the DFIG system will oscillate due to insufficient phase margin, indicating that the DFIG-grid interconnected system will have some resonance issues at 275 Hz.

The equivalent SISO impedance of the DFIG system that defines the system delay matrix $\boldsymbol{K}_m$ as an identity matrix to ignore the system delay is also drawn in Fig. 6. There is no interaction between the amplitude–frequency characteristic curve of equivalent SISO impedance for DFIG and the grid impedance (SCR = 2). The phase of the DFIG system is 0° at 100 Hz, and the phase–frequency characteristic curve of equivalent SISO impedance for DFIG continues to rise as the frequency increases, which means that the DFIG-grid interconnected system keeps

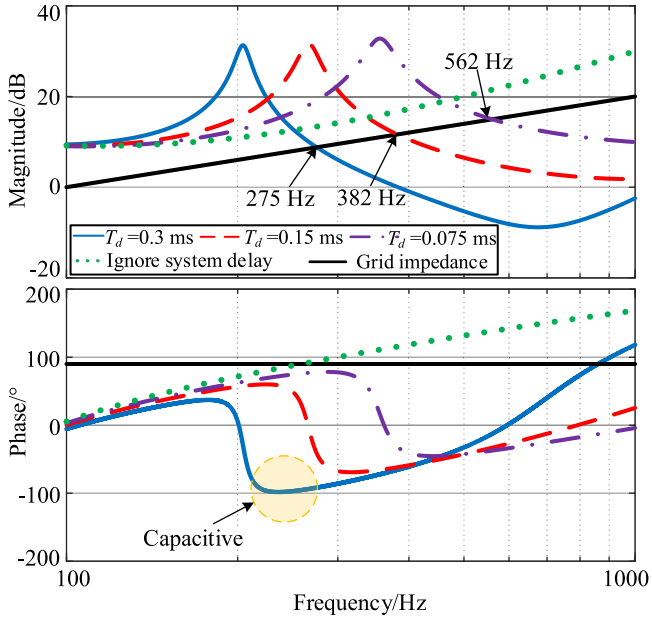

Fig. 6. Bode diagram of equivalent SISO impedance for DFIG based on DPC with system delay variations (SCR = 2).

sufficient phase margin at high frequency. Therefore, the DFIG system based on DPC is stable under inductive weak grid at high frequency when the system delay is ignored.

The type of HFR in this article is different from those in [9] and [17]. The scenario of HFR occurs in [9] and [17] is that the DFIG system has insufficient phase margin when connected to the parallel-compensated grid, since the DFIG system behaves as an inductance at high frequency while the parallel-compensated grid will behave as a capacitance. However, this article analyzes the HFR of DFIG system under the inductive weak grid rather than parallel-compensated grid. It is interesting to analyze the mechanism of this HFR, and the reason why the DFIG is not inductive at high frequency while employing the DPC.

C. Existing System Delay Compensation Strategy

According to Section IV-B, the system delay will influence the impedance characteristics of DFIG system at high frequency, which will introduce some stability problem. Therefore, compared with the DFIG system based on conventional vector control, it is more necessary to compensate the system delay for the DFIG system based on DPC. An existing system delay compensation strategy by adding a leading phase compensator to counteract the system delay matrix $\boldsymbol{K}_m$ within a specific frequency range is proposed in [29], which is shown as follows:

$$\boldsymbol{G}_{com} = \begin{bmatrix} e^{jn\omega_g T_d} & 0 \\ 0 & e^{(jn\omega_g - 2j\omega_g)T_d} \end{bmatrix}. \tag{17}$$

The Bode diagram of equivalent SISO impedance for DFIG with the existing system delay compensation strategy is shown in Fig. 7. The compensation frequency band can be adjusted by changing compensation factor n. As the compensation factor n increases from 3 to 12, it can be found that the intersection of the amplitude–frequency characteristic curve will move to higher

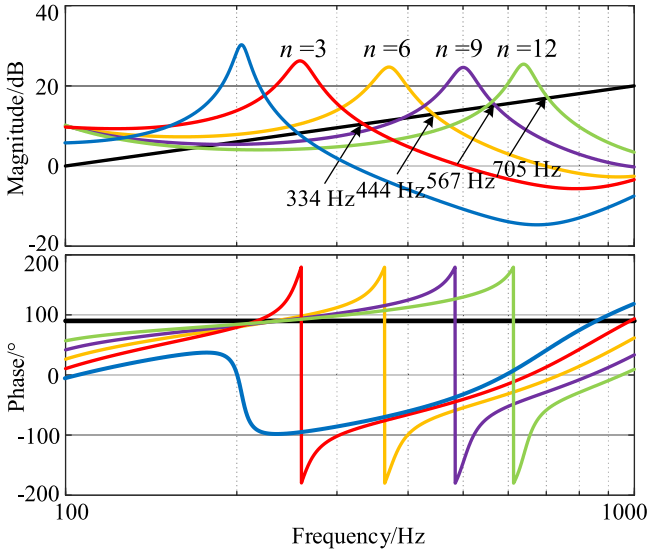

Fig. 7. Bode diagram of equivalent SISO impedance for DFIG with the existing system delay compensation strategy (SCR = 2).

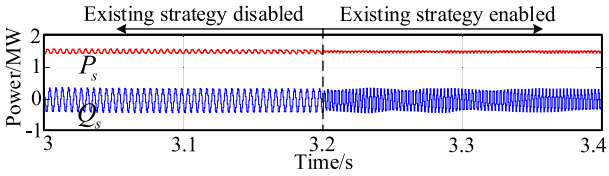

Fig. 8. Resonance phenomenon after employing the existing system delay compensation strategy.

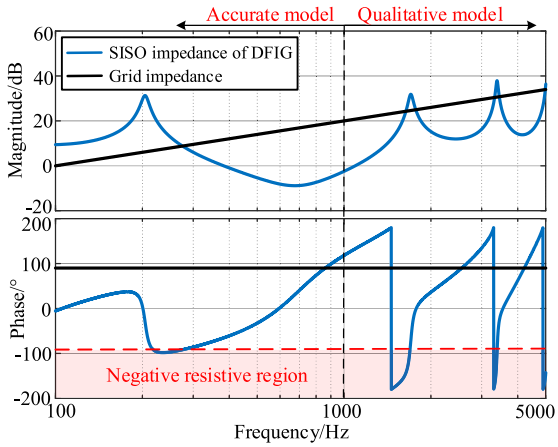

Fig. 9. Further analysis of equivalent SISO impedance at high frequency.

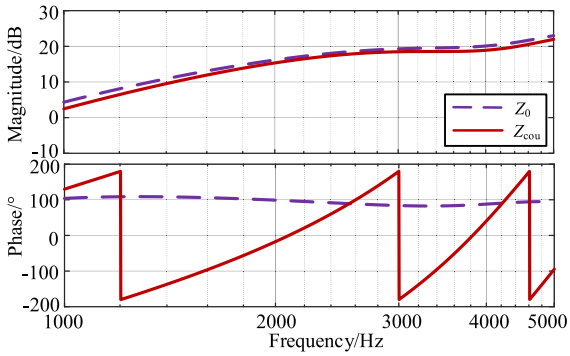

Fig. 10. Bode diagram of impedance subsystems Z_0 and Z_{cou}.

frequencies from 334 to 705 Hz. Nevertheless, the DFIG system still has a strong capacitance or even a negative resistance at the frequency of intersections. The simulation results after enabling the existing system delay compensation strategy (compensation factor $n = 6$) is shown in Fig. 8. It can be found that the resonant frequency is shifted to 344 and 444 Hz, whereas the resonance problem has not been solved. Therefore, the resonance issues cannot be eliminated after employing the existing system delay compensation strategy. It is of importance to further analyze the mechanism of the HFR and propose an improved reshaping control strategy.

V. Further Analysis of High-Frequency Characteristics and Reshaping Control Strategy

A. Further Discussion for the High-Frequency Impedance

In order to further analyze the cause of HFR to compensate for the resonance issues, Fig. 9 depicts the equivalent SISO impedance for the DFIG system from 100 to 5000 Hz. Actually, the impedance characteristics between 2500 and 5000 Hz will be affected by modulation, so that we cannot accurately predict the resonance frequency above 2500 Hz. However, the Bode diagram of equivalent SISO impedance above 2500 Hz can also qualitatively reflect the changing trend of impedance characteristics to further study the mechanism of HFR.

It can be noticed that, as the frequency continues to increase, the amplitude–frequency characteristic curves of the DFIG system and grid impedance will intersect multiple times at high frequency. The DFIG system behaves as a negative resistance periodically, which will deteriorate the stability of the DFIG system at high frequency for DPC.

When the frequency exceeds 1000 Hz, the amplitude of s is much greater than ω_r and $2\omega_g$. Therefore, (13) can be further simplified as

$$\boldsymbol{Y}_{\mathrm{DFIG}} = \begin{bmatrix} Y_{11} & Y_{12} \\ Y_{21} & Y_{22} \end{bmatrix} \approx \begin{bmatrix} \frac{1}{sL_r\sigma+1.5K_pe^{-sT_d}} & \frac{-1.5K_p\boldsymbol{I}_{s1}e^{-sT_d}/U_{sd1}}{sL_r\sigma+1.5K_pe^{-sT_d}} \\ \frac{-1.5K_p\boldsymbol{I}_{s1}^{*}e^{-sT_d}/U_{sd1}}{sL_r\sigma+1.5K_pe^{-sT_d}} & \frac{1}{sL_r\sigma+1.5K_pe^{-sT_d}} \end{bmatrix}. \tag{18}$$

According to (18), several conclusions can be reached as follows.

First, it can be found that $Y_{11} \approx Y_{22}$ and $Y_{12} \approx Y_{21}$ above 1000 Hz. These four elements of DFIG admittance have the same denominator and all contain the components of system delay e^{-sTd}. Note that e^{-sTd} is an element whose amplitude is constant at 1 while the phase will change periodically. Compared with $sL_r\sigma$, the components of system delay e^{-sTd} can be ignored at high frequency due to the limited amplitude. Fig. 10 depicts

the Bode diagram of the impedance subsystem $Z_0 = 1/Y_{11}$ that does not consider the frequency coupling characteristic. The phase of Z_0 is 90° with slight fluctuations and the high-frequency characteristic is similar to the DFIG system based on conventional vector control, which is inductive above the bandwidth of controller.

Second, by comparison with Y_{11} and Y_{22}, the off-diagonal elements Y_{12} and Y_{21} also contain the components of system delay e^{-sTd} in numerator, which may cause the phase to change periodically at high frequency. Due to the fact that the impedance subsystem Z_{cou} introduced by frequency coupling characteristic will be affected by Y_{12} and Y_{21}, the Bode diagram of Z_{cou} is also drawn in Fig. 10. From Fig. 10, it is verified that the phase of Z_{cou} will change periodically and Z_{cou} behaves as a negative resistance at high frequency. In addition, the amplitude of the amplitude–frequency characteristic curve of Z_0 is approximated to Z_{cou} above 1000 Hz, thus the frequency characteristics of the DFIG system based on DPC is decided by Z_0 and Z_{cou} together.

In conclusion, a strong frequency coupling related to the components of system delay e^{-sTd} will influence the high-frequency characteristics of the DFIG system, and the periodic change of phase introduced by the system delay will cause some resonance issues for the DFIG system with DPC at high frequency.

Due to the limited bandwidth of existing system delay compensation strategy, it cannot compensate the system delay in the whole high-frequency range, thus the negative resistance will still exist as shown in Fig. 7. Since the negative effects of system delay are mainly in the off-diagonal elements Y_{12} and Y_{21}, it is possible to suppress the periodic change of phase by canceling the frequency coupling characteristic at high frequency, thereby eliminating resonance.

In addition, since e^{-sTd} is multiplied by the proportional gain K_p according to (18), the negative impact of system delay will be more significant with larger K_p.

The conclusions of PI-DPC in this article are also applicable to GVM-DPC, since the GVM-DPC also employs the PI controller in a two-phase stationary reference, whose high-frequency impedance characteristics is similar to the PI-DPC. However, the conclusions obtained by PI-DPC cannot be fully applied to SMC-DPC and MPC-DPC, because the SMC-DPC and MPC-DPC, respectively, employ the sliding mode controller and the cost function rather than PI controller to track the reference output power. Nevertheless, according to this article, there is a tradeoff between the fast dynamic response and the potential risk of high-frequency instability after employing the PI-DPC, which may have the certain reference significance for the subsequent SMC-DPC and MPC-DPC analyses.

B. Design of the Impedance Reshaping Control Strategy

According to (13), the matrices in the admittance of the DFIG system based on DPC at high frequency are all diagonal matrices except $\boldsymbol{G}_{pni}$. The off-diagonal $\boldsymbol{G}_{pni}$ introduced by power calculation will cause the positive and negative sequence impedances no longer decoupled, which may bring strong frequency coupling characteristics. The basic idea to suppress the frequency coupling characteristic is introducing a virtual impedance $\boldsymbol{Z}_v$ to counteract $\boldsymbol{G}_{pni}$ at high frequency, which is shown in Fig. 11,

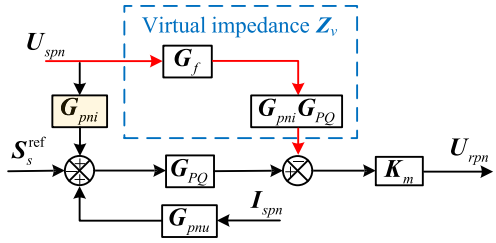

Fig. 11. Impedance reshaping control strategy based on virtual impedance.

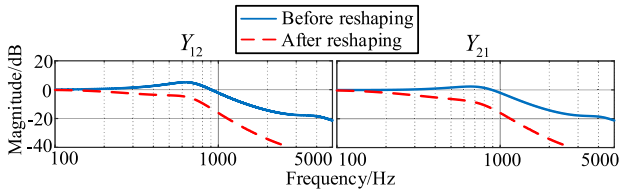

Fig. 12. Amplitude–frequency characteristic curves of off-diagonal elements in the DFIG impedance model with virtual impedance.

According to Fig. 11, the proposed virtual impedance $\boldsymbol{Z}_v$ is composed of the phase compensation controller $\boldsymbol{G}_{pni}\boldsymbol{G}_{PQ}$ and the high-pass filter $\boldsymbol{G}_f$. The cutoff frequency of filter $\boldsymbol{G}_f$ is fixed at 200 Hz ($\omega_L = 2\pi \cdot 200$) to avoid affecting the fundamental frequency. The virtual impedance in this article is different from those in [9] and [17]. The virtual impedance in [9] and [17] only has the diagonal elements, whose purpose is to reduce the phase difference between the DFIG and the parallel-compensated grid at the intersection of amplitude–frequency characteristic curves. However, the virtual impedance in this article contains the off-diagonal elements, which can reduce the degree of frequency coupling at high frequency to suppress the periodic negative resistance introduced by system delay

$$\boldsymbol{Z}_v = \begin{bmatrix} 0 & \frac{1.5\boldsymbol{I}_{s1}H_{pi}(s)s}{s+\omega_L} \\ \frac{1.5\boldsymbol{I}_{s1}^{*}H_{pi}(s)s}{s+\omega_L} & 0 \end{bmatrix}. \tag{19}$$

The amplitude–frequency characteristic curves of off-diagonal elements Y_{12} and Y_{21} are depicted in Fig. 12, and the degree of frequency coupling is reduced after employing the proposed impedance reshaping control strategy, which simplifies the impedance model of the DFIG system based on DPC at high frequency.

Fig. 13 depicts the Bode diagram of equivalent SISO impedance for DFIG after adding the virtual impedance. The amplitude–frequency characteristic curve of the equivalent SISO impedance for DFIG and the grid impedance intersect at 185 Hz after reshaping according to Fig. 13. The difference of phase decreases from 182° to 128°, indicating that the resonance issues are eliminated due to the sufficient phase margin. In addition, there is no interaction of the amplitude–characteristic curve any more between the equivalent SISO impedance for DFIG and the grid as the frequency continues to increase. The DFIG system behaves as an inductance rather than a periodically changing negative resistance, which can cancel the potential risk of instability.

Fig. 14 shows the Bode diagram of equivalent SISO impedance after reshaping when SCR is 2.6, 2, and 1.6, and

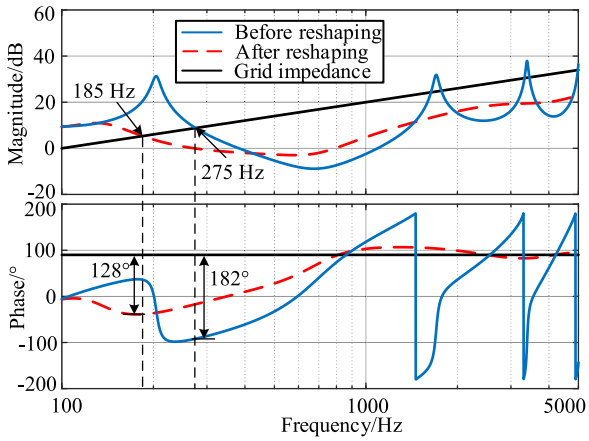

Fig. 13. Bode diagram of equivalent SISO impedance for DFIG with virtual impedance (SCR = 2).

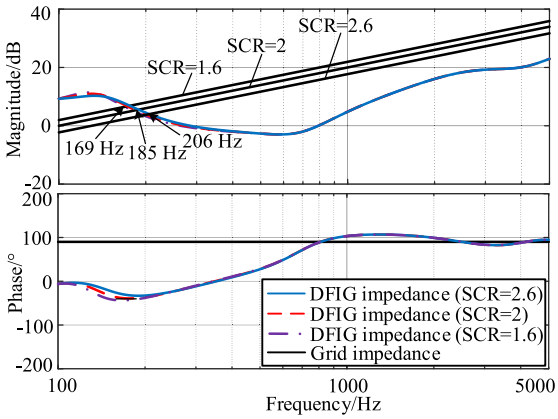

Fig. 14. Bode diagram of equivalent SISO impedance for DFIG after employing the proposed reshaping control strategy with SCR deviations.

it can be found that the amplitude–frequency characteristic curves of the equivalent SISO impedance for DFIG and the grid impedance intersect at 206, 185, and 169 Hz, respectively. The DFIG-grid interconnected system has a sufficient phase margin with different SCR, which validates the robustness against SCR deviations of the proposed impedance reshaping control strategy. Note that there is a slight difference in the DFIG impedance when SCR changes. The reason lies in the fact that the reshaping control strategy does not completely eliminate the frequency coupling characteristics, so the equivalent SISO impedance of the DFIG system will still be related to negative sequence grid impedance according to Fig. 5.

VI. Experimental Results

If the real plant for experimental evaluation based on the small-scaled laboratory setup of kW class DFIG is carried out, it is difficult to simulate the impedance characteristics of megawatt DFIG-based wind energy conversion systems, since the DFIG parameters are reduced correspondingly with the power level. To further verify the effectiveness of the proposed impedance reshaping control strategy, the hardware platform is established based on control-hardware-in-loop (CHIL) as shown in Fig. 15.

Fig. 15. Hardware platform of CHIL experiment.

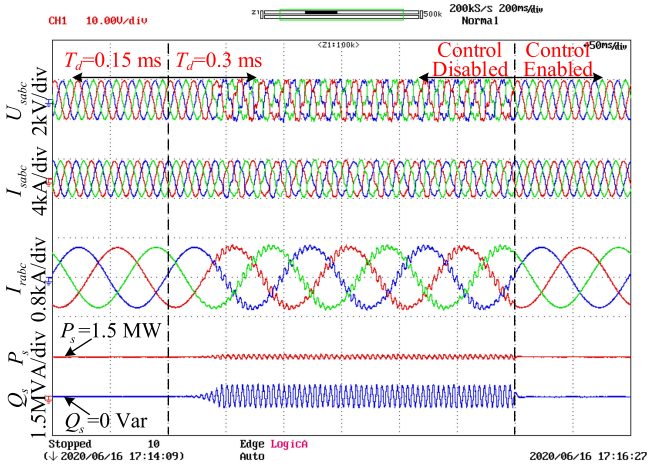

Fig. 16. Experimental results of HFR with different system delay and the validation of proposed reshaping control strategy.

The model of DFIG system is developed in Typhoon 602+ with the time step of 1 μs. The controllers of DFIG are implemented in a TMS320F28335/Spartan6 XC6SLX16 DSP+FPGA control board. Applying the CHIL to analyze the stability of megawatt DFIG-grid interconnected system has also been proposed in [8] and [10].

The reference output active and reactive powers of the DFIG system are 1.5 MW and 0 Var. The other parameters of DFIG are the same as the simulations, which are listed in Table I. Fig. 16 depicts the experimental results of HFR with different system delay and the validation of proposed reshaping control strategy. The DFIG system based on DPC has some resonance issues when the system delay T_d changes from 0.15 to 0.3 ms by adding some extra delay link before modulation. According to fast Fourier transform (FFT) analysis as shown in Fig. 17, the DFIG-grid interconnected system will oscillate at 275 and 175 Hz, which is the same as the analysis results in Fig. 6. The total harmonic distortion (THD) of the stator voltage $\boldsymbol{U}_s$ and current $\boldsymbol{I}_s$ are 19.88% and 13.33%. The THD of stator voltage $\boldsymbol{U}_s$ and current $\boldsymbol{I}_s$ are reduced to 1.02% and 1.06% after enabling the proposed reshaping control strategy, which indicate that the proposed reshaping control strategy can improve the stability of the DFIG system based on DPC when the system delay increases.

The proposed impedance reshaping control strategy has little impact on the dynamic power tracking ability of DPC as shown in Fig. 18 due to the high-pass filter in the virtual impedance.

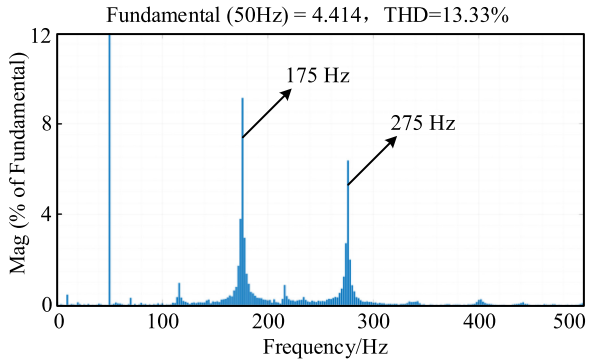

Fig. 17. FFT analysis of stator current.

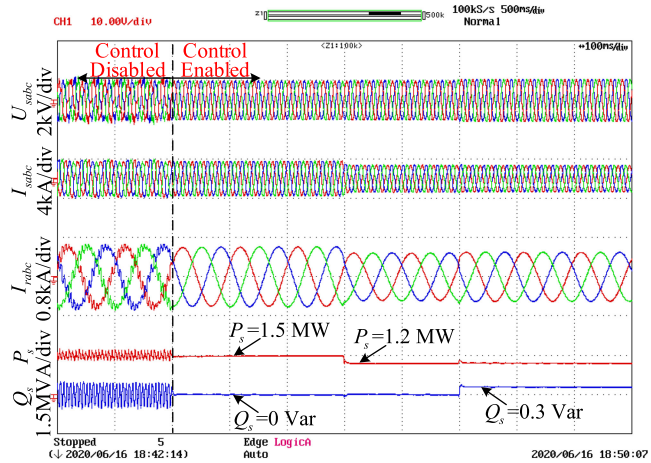

Fig. 18. Dynamic power tracking ability of the DFIG system after enabling the proposed impedance reshaping control strategy.

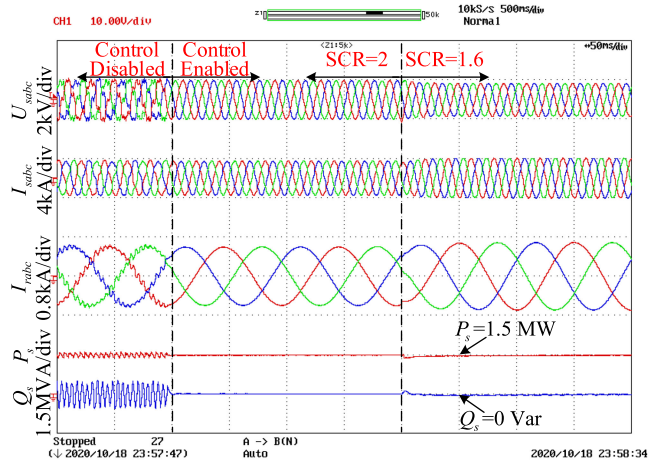

Fig. 19. Experimental results with SCR deviations.

The reference of stator active power P_s and reactive power Q_s decreases from 1.5 to 1.2 MW and increases from 0 to 0.3 MVar, respectively, after enabling the proposed reshaping control strategy, and the DFIG system still has the fast dynamic power tracking ability to take a short response time of around 10 ms.

The experiment results in Fig. 19 also show that after the SCR is changed from 2 to 1.6, the DFIG system will be stable after a slight oscillation.

Note that there is a coupling between P_s and Q_s according to Figs. 18 and 19. It can further analyze whether this reshaping controller can be applied to other improved types of DPC, such as GVM-DPC, which can achieve the fast dynamic response capability and sufficient high-frequency phase margin at the same time.

VII. Conclusion

This article analyzes the impedance characteristics of a DFIG system based on DPC under inductive weak grid. The specific contribution of this article can be concluded as follows.

1) The off-diagonal $\boldsymbol{G}_{pni}$ introduced by power calculation will cause the positive and negative sequence impedances no longer decoupled. Therefore, the established impedance model is a MIMO model with a strong frequency coupling at high frequency, which complicates the stability analysis.
2) The system delay will influence the numerator in off-diagonal admittance, and the DFIG system will behave as a capacitance or negative resistance periodically. As the system delay increases, DFIG-grid interconnected system will not have sufficient phase margin, resulting in HFR issues.
3) An impedance reshaping control strategy that counteracts the off-diagonal matrix $\boldsymbol{G}_{pni}$ is proposed to reduce the degree of frequency coupling at high frequency, for eliminating the negative effects of system delay and suppressing the HFR. The proposed impedance reshaping control strategy has the robustness against SCR deviations, and will not affect the fast dynamic power tracking ability of DPC.

References

[1] F. Blaabjerg, M. Liserre, and K. Ma, "Power electronics converters for wind turbine systems," *IEEE Trans. Ind. Appl.*, vol. 48, no. 2, pp. 708–719, Mar./Apr. 2012.
[2] H. Polinder, J. A. Ferreira, B. B. Jensen, A. B. Abrahamsen, K. Atallah, and R. A. McMahon, "Trends in wind turbine generator systems," *IEEE J. Emerg. Sel. Topics Power Electron.*, vol. 1, no. 3, pp. 174–185, Sep. 2013.
[3] S. Muller, M. Deicke, and R. W. De Doncker, "Doubly fed induction generator systems for wind turbines," *IEEE Ind. Appl. Mag.*, vol. 8, no. 3, pp. 26–33, May/Jun. 2002.
[4] I. Vieto and J. Sun, "Sequence impedance modeling and analysis of type-III wind turbines," *IEEE Trans. Energy Convers.*, vol. 33, no. 2, pp. 537–545, Jun. 2018.
[5] X. Xi, H. Geng, and Y. Geng, "Enhanced model of the doubly fed induction generator-based wind farm for small-signal stability studies of weak power system," *IET Renew. Power Gener.*, vol. 8, no. 7, pp. 765–774, Jul. 2014.
[6] C. Zhang, X. Cai, M. Molinas, and A. Rygg, "Frequency-domain modelling and stability analysis of a DFIG-based wind energy conversion system under non-compensated AC grids: Impedance modelling effects and consequences on stability," *IET Power Electron*, vol. 12, no. 4, pp. 907–914, Apr. 2019.
[7] J. Hu, Y. Huang, D. Wang, H. Yuan, and X. Yuan, "Modeling of grid-connected DFIG-based wind turbines for DC-link voltage stability analysis," *IEEE Trans. Sustain. Energy.*, vol. 6, no. 4, pp. 1325–1336, Oct. 2015.

[8] K. Sun, W. Yao, J. Fang, X. Ai, J. Wen, and S. Cheng, "Impedance modeling and stability analysis of grid-connected DFIG-based wind farm with a VSC-HVDC," *IEEE J. Emerg. Sel. Topics Power Electron.*, vol. 8, no. 2, pp. 1375–1390, Jun. 2020.
[9] Y. Song and F. Blaabjerg, "Overview of DFIG-based wind power system resonances under weak networks," *IEEE Trans. Power Electron.*, vol. 32, no. 6, pp. 4370–4394, Jun. 2017.
[10] W. Liu, X. Xie, X. Zhang, and X. Li, "Frequency-coupling admittance modeling of converter-based wind turbine generators and the control-hardware-in-the-loop validation," *IEEE Trans. Energy Convers.*, vol. 35, no. 1, pp. 425–433, Mar. 2020.
[11] X. Wang, L. Harnefors, and F. Blaabjerg, "Unified impedance model of grid-connected voltage-source converters," *IEEE Trans. Power Electron.*, vol. 33, no. 2, pp. 1775–1787, Feb, 2018.
[12] A. Rygg, M. Molinas, C. Zhang, and X. Cai, "A modified sequence domain impedance definition and its equivalence to the dq-domain impedance definition for the stability analysis of ac power electronic systems," *IEEE J. Emerg Sel. Topics Power Electron.*, vol. 4, no. 4, pp. 1383–1396, Dec. 2016.
[13] J. Sun, "Impedance-based stability criterion for grid-connected inverters," *IEEE Trans. Power Electron.*, vol. 26, no. 11, pp. 3075–3078, Nov. 2011.
[14] H. Liu, X. Xie, Y. Li, H. Liu, and Y. Hu, "Mitigation of SSR by embedding subsynchronous notch filters into DFIG converter controllers," *IET Gener. Transmiss. Distrib.*, vol. 11, no. 11, pp. 2888–2896, Sep. 2017.
[15] Y. Xu, H. Nian, T. Wang, L. Chen, and T. Zheng, "Frequency coupling characteristic modeling and stability analysis of doubly fed induction generator," *IEEE Trans. Energy Convers.*, vol. 33, no. 3, pp. 1475–1486, Sep. 2018.
[16] A. E. Leon, "Integration of DFIG-based wind farms into series-compensated transmission systems," *IEEE Trans. Sustain. Energy.*, vol. 7, no. 2, pp. 451–460, Apr. 2016.
[17] H. Nian and B. Pang, "Stability and power quality enhancement strategy for DFIG system connected to harmonic grid with parallel compensation," *IEEE Trans. Energy Convers.*, vol. 34, no. 2, pp. 1010–1022, Jun. 2019.
[18] C. Zou *et al.*, "Analysis of resonance between a VSC-HVDC converter and the AC grid," *IEEE Trans. Power Electron.*, vol. 33, no. 12, pp. 10157–10168, Dec. 2018.
[19] L. Xu and L. Fan, "Impedance-Based resonance analysis in a VSC-HVDC system," *IEEE Trans. Power Del.*, vol. 28, no. 4, pp. 2209–2216, Oct. 2013.
[20] L. Shang and J. Hu, "Sliding-mode-based direct power control of grid-connected wind-turbine-driven doubly fed induction generators under unbalanced grid voltage conditions," *IEEE Trans. Energy Convers.*, vol. 27, no. 2, pp. 362–373, Jun. 2012.
[21] S. Aurtenechea Larrinaga, M. A. Rodriguez Vidal, E. Oyarbide, and J. R. Torrealday Apraiz, "Predictive control strategy for DC/AC converters based on direct power control," *IEEE Trans. Ind. Electron.*, vol. 54, no. 3, pp. 1261–1271, Jun. 2007.
[22] Y. Gui, C. Kim, C. C. Chung, J. M. Guerrero, Y. Guan, and J. C. Vasquez, "Improved direct power control for grid-connected voltage source converters," *IEEE Trans. Ind. Electron.*, vol. 65, no. 10, pp. 8041–8051, Oct. 2018.
[23] S. Gao, H. Zhao, Y. Gui, D. Zhou, and F. Blaabjerg, "An improved direct power control for doubly fed induction generator," *IEEE Trans. Power Electron.*, vol. 36, no. 4, pp. 4672–4685, Apr. 2021.
[24] H. Nian and L. Li, "Direct power control of doubly fed induction generator without phase-locked loop under harmonically distorted voltage conditions," *IEEE Trans. Power Electron.*, vol. 33, no. 7, pp. 5836–5846, Jul. 2018.
[25] B. Hu, H. Nian, M. Li, and Y. Xu, "Impedance characteristic analysis and reshaping method of DFIG system based on DPC without PLL," *IEEE Trans. Ind. Electron.*, to be published, doi: 10.1109/TIE.2020.3028826.
[26] W. Liu, X. Xie, X. Zhang, and X. Li, "Frequency-coupling admittance modeling of converter-based wind turbine generators and the control-hardware-in-the-loop validation," *IEEE Trans. Energy Convers.*, vol. 35, no. 1, pp. 425–433, Mar. 2020.
[27] C. Zhang, X. Cai, A. Rygg, and M. Molinas, "Sequence domain SISO equivalent models of a grid-tied voltage source converter system for small-signal stability analysis," *IEEE Trans. Energy Convers.*, vol. 33, no. 2, pp. 741–749, Jun. 2018.
[28] S. Gao, H. Zhao, Y. Gui, J. Luo, and F. Blaabjerg, "Impedance analysis of voltage source converter using direct power control," *IEEE Trans. Energy Convers.*, to be published, doi: 10.1109/TPC.2020.3020181.
[29] C. Wu and H. Nian, "Stator harmonic currents suppression for DFIG based on feed-forward regulator under distorted grid voltage," *IEEE Trans. Power Electron.*, vol. 33, no. 2, pp. 1211–1224, Feb. 2018.

Bin Hu was born in Wenzhou, China. He received the B.Eng. degree in electrical engineering from Shenyang University of Technology, Shenyang, China, in 2018. He is currently working toward the Ph.D. degree in electrical engineering with Zhejiang University, Hangzhou, China.

His research interests include the phase-locked synchronization methods for wind power generation systems under weak grid, their impedance characteristic analysis, and reshaping control strategy.

Heng Nian (Senior Member, IEEE) received the B.Eng. and M.Eng. degrees from Hefei University of Technology, Hefei, China, in 1999 and 2002, respectively, and the Ph.D. degree from Zhejiang University, Hangzhou, China, in 2005, all in electrical engineering.

From 2005 to 2007, he was a Postdoctoral with the College of Electrical Engineering, Zhejiang University, where he was promoted to an Associate Professor in 2007. Since 2016, he has been a Full Professor of electrical engineering with the College of Electrical Engineering, Zhejiang University. From 2013 to 2014, he was a Visiting Scholar with the Department of Electrical, Computer, and System Engineering, Rensselaer Polytechnic Institute, Troy, NY, USA. He has authored or coauthored more than 40 IEEE/IET transaction papers and holds more than 20 issued/pending patents. His current research interests include the optimal design and operation control for wind power generation systems.

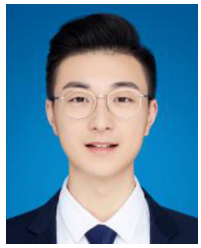

Jun Yang was born in Wenzhou, China. He received the B.Eng. degree in electrical engineering in 2019 from Zhejiang University, Hangzhou, China, where he is currently working toward the M.Eng. degree in electrical engineering.

His research interests include the impedance-based stability analysis methods for ac–dc hybrid power systems under weak ac grid and corresponding impedance reshaping control strategy.

Meng Li was born in Chifeng, China. He received the B.Eng. degree in electrical engineering in 2019 from Zhejiang University, Hangzhou, China, where he is currently working toward the Ph.D. degree in electrical engineering.

His research interests include small-signal stability analysis of grid-connected operation and the technology for impedance measurement of renewable generators.

Yunyang Xu (Graduate Student Member, IEEE) was born in Deyang, China. She received the B.Eng. degree in electrical engineering in 2016 from Zhejiang University, Hangzhou, China, where she is currently working toward the Ph.D. degree in electrical engineering.

Her research interests include small-signal modeling of renewable generators, their integration to the electric grid, and system stability analysis.